COMMUNICATIONS IN COMPUTATIONAL PHYSICS
Vol. **2**, No. 4, pp. 723-745

Commun. Comput. Phys.
August 2007

Multiscale Finite Element Modelling of Flow Through Porous Media with Curved and Contracting Boundaries to Evaluate Different Types of Bubble Functions

V. Nassehi[1,*], M. Parvazinia[2] and A. Khan[1]

[1] *Department of Chemical Engineering, Loughborough University, Loughborough, Leicestershire, LE11 3TU, UK.*

[2] *Department of Mathematical Modelling and Simulation, Iran Polymer and Petrochemical Institute, Tehran, P.O. Box 14185/458, Iran.*

Received 15 August 2006; Accepted (in revised version) 9 November 2006

Communicated by Pingwen Zhang

Available online 22 January 2007

Abstract. The Brinkman equation is used to model the isothermal flow of the Newtonian fluids through highly permeable porous media. Due to the multiscale behaviour of this flow regime the standard Galerkin finite element schemes for the Brinkman equation require excessive mesh refinement at least in the vicinity of domain walls to yield stable and accurate results. To avoid this, a multiscale finite element method is developed using bubble functions. It is shown that by using bubble enriched shape functions the standard Galerkin method can generate stable solutions without excessive near wall mesh refinements. In this paper the performances of different types of bubble functions are evaluated. These functions are used in conjunction with bilinear Lagrangian elements to solve the Brinkman equation via a penalty finite element scheme.

PACS (2006): 47.11.-j, 47.11.Fg, 47.11.St

Key words: Finite element, multiscale method, porous media, Newtonian fluid flow, bubble function, static condensation.

1 Introduction

In a porous medium, flow can be represented by different types of governing equations depending on the range of the permeability of the domain and the flow Reynolds number [1]. In highly permeable porous media, low Reynolds number flow regimes can be

*Corresponding author. *Email addresses:* V.Nassehi@lboro.ac.uk (V. Nassehi), A.Khan@lboro.ac.uk (M. Parvazinia), m.parvazinia@ippi.ac.ir (A. Khan)

represented by the Brinkman equation. In this type of flow where permeability of porous matrix is high the fluid carries some of the imposed stress. This effect rises sharply in near wall layers as the permeability of porous media decreases. It is interpreted as the flow system having different scales, a "fine scale" in the near wall zone and a "coarse scale" in the rest of the domain. Therefore, theoretically accurate modelling of the Brinkman regime can only be obtained via excessive mesh refinement of the solution domain, at least in the region of the boundary layer [2]. However, the thickness of the boundary layer is not known a priori and depends on the domain permeability. This in turn makes the classical schemes such as the standard Galerkin method unsuitable for a multiscale problem such as the Brinkman equation [3]. These types of problems can be modelled using multiscale variational methods [4, 5]. These techniques are currently used to solve problems related to turbulent flows, structural analysis of composite materials, flow through porous media, weather forecasting and large-scale molecular dynamic simulations. Representation of all physical scales need a high level of discretisation which is a common difficulty with these problems. To have stable-accurate solution, the multiscale method should be capable of incorporating the influence of the fine-scales while using discretisation at a coarse level to avoid excessive mesh refinement. In a two-scale method, the field unknown is divided into two parts as $u = u_1 + u_b$, where u_b is known as fine, sub-grid or unresolved scale which may be derived analytically and u_1 is known as coarse or resolved scale where is represented by a standard polynomial finite element approximation.

In spite of theoretical progresses in this area the development of algorithms which enable implementation of the theoretical considerations in practice is not a trivial matter [6]. Bubble functions can be incorporated in a finite element discretisation to generate a multiscale scheme. These functions are, typically, high order polynomials which vanish on the element boundaries [7–11]. The bubble functions can be systematically derived using the residual free bubble method [12–15]. The essential idea of this method is that the bubble functions should satisfy, strongly, the model differential equation within each element subject to homogeneous boundary conditions. In multi-dimensional problems, the analytical solution of a partial differential equation (PDE) in the residual free method within each element is a major task. The analytical solution of a PDE can be replaced by the analytical solution of an ODE (ordinary differential equation), in the residual free bubble function method. To this end the exact solution of the ODE is approximated by the Taylor series expansion and the multi-dimensional bubble functions are derived by tensor product of one dimensional bubbles.

In the present work, a continuous penalty scheme is used to evaluate polynomial bubble functions in multiscale finite element solution of the flow in porous media with curved and contracting boundaries using the Brinkman equation. The method of incorporating bubble functions with Lagrangian shape functions using static condensation method, derivation of two dimensional bubble functions and elimination of the boundary integrals are explained. The numerical results are validated with analytical solution in a simple rectangular domain and then the isothermal flow of a Newtonian fluid is studied in different domains.

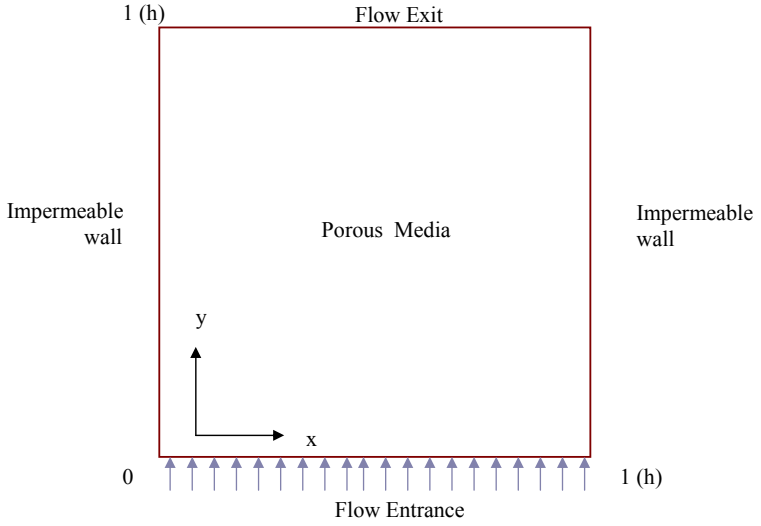

Figure 1: Rectangular flow domain (domain 1) and boundaries used for model validation.

2 Governing equations

The governing equations of isothermal flow of Newtonian fluids in a porous duct with impermeable walls (Fig. 1) in a two dimensional Cartesian coordinate system are given by:
Continuity equation:

$$\frac{\partial u}{\partial x}+\frac{\partial v}{\partial y}=0, \tag{2.1}$$

x-component of the Brinkman equation:

$$-\frac{\partial p}{\partial x}-\frac{\mu}{K}u+\mu_e\left(\frac{\partial^2 u}{\partial x^2}+\frac{\partial^2 u}{\partial y^2}\right)=0, \tag{2.2}$$

y-component of the Brinkman equation:

$$-\frac{\partial p}{\partial y}-\frac{\mu}{K}v+\mu_e\left(\frac{\partial^2 v}{\partial x^2}+\frac{\partial^2 v}{\partial y^2}\right)=0, \tag{2.3}$$

where u and v are velocity components, p is pressure, μ is fluid viscosity, K is the domain permeability and μ_e is the effective viscosity that theoretically takes into account the stress borne by the fluid as it flows through a porous medium. However, experimental measurement of μ_e is not a trivial matter, if not impossible [1]. Therefore, in the present work in accordance with overwhelming majority of the published literatures μ_e is set to be equal to the fluid viscosity μ, e.g., [16–18].

2.1 Boundary conditions

We use the following boundary conditions (see Fig. 1):

(i). Inlet to the domain
In accordance with majority of engineering flow processes at the inlet a plug flow condition is applied. This can be written as follows:

$$u=0, \quad v=v_0 \qquad \text{for} \quad 0<x<h \quad \text{and} \quad y=0, \tag{2.4}$$

where h is the gap width in a rectangular domain.

(ii). At impermeable (solid) walls

$$\begin{aligned} &u=0, \quad v=0 \qquad \text{for} \quad x=0 \quad \text{and} \quad 0\leq y<h, \\ &u=0, \quad v=0 \qquad \text{for} \quad x=h \quad \text{and} \quad 0\leq y<h. \end{aligned} \tag{2.5}$$

(iii). Exit
At the outlet a stress free condition is used, therefore both shear and normal components of the surface forces are set to zero:

$$\tau_{yy}\big|_{exit}=2\mu\frac{\partial v}{\partial y}=0 \qquad \text{for } y=h,\ 0\leq x\leq h, \tag{2.6}$$

$$\tau_{yx}\big|_{exit}=\tau_{xy}\big|_{exit}=\mu\left(\frac{\partial u}{\partial y}+\frac{\partial v}{\partial x}\right)=0 \qquad \text{for } y=h,\ 0\leq x\leq h, \tag{2.7}$$

$$\tau_{xx}\big|_{exit}=2\mu\frac{\partial u}{\partial x}=0 \qquad \text{for } y=h,\ 0\leq x\leq h. \tag{2.8}$$

The use of "stress free" instead of "developed flow" conditions provides a more general exit boundary condition enabling the simulation of realistic situations where the flow development cannot be guaranteed.

2.2 Dimensionless form of the governing equations

To preserve the consistency of the numerical solutions we use the following dimensionless variables [2]:

$$\begin{aligned} &y^*=\frac{y}{h}, \quad x^*=\frac{x}{h}, \quad u^*=\frac{u\mu}{\rho gh^2}, \quad v^*=\frac{v\mu}{\rho gh^2}, \quad p^*=\frac{p}{\rho gh}, \\ &\tau_{xx}^*=\frac{\tau_{xx}}{\rho gh}, \quad \tau_{yy}^*=\frac{\tau_{yy}}{\rho gh}, \quad \tau_{yx}^*=\frac{\tau_{yx}}{\rho gh}, \quad \tau_{xy}^*=\frac{\tau_{xy}}{\rho gh}, \end{aligned}$$

where ρ is the fluid density, p is the pressure and g is acceleration due to gravity. Substituting the defined dimensionless variables in Eqs. (2.1)-(2.8) the following dimensionless

governing equations are obtained:

$$\frac{\partial u^*}{\partial x^*}+\frac{\partial v^*}{\partial y^*}=0, \tag{2.9}$$

$$-\frac{\partial p^*}{\partial x^*}-\frac{1}{Da}u^*+\left(\frac{\partial^2 u^*}{\partial x^{*2}}+\frac{\partial^2 u^*}{\partial y^{*2}}\right)=0, \tag{2.10}$$

$$-\frac{\partial p^*}{\partial y^*}-\frac{1}{Da}v^*+\left(\frac{\partial^2 v^*}{\partial x^{*2}}+\frac{\partial^2 v^*}{\partial y^{*2}}\right)=0, \tag{2.11}$$

where Da is the Darcy parameter defined as:

$$Da=K/h^2.$$

The corresponding dimensionless boundary conditions are expressed as:

(i). Entrance

$$u^*=0, \quad v^*=v_0^* \qquad \text{for} \quad y=0,\ 0<x<1. \tag{2.12}$$

In this work v_0^* was selected to be equal to 0.01. This is to assure that the flow regime remains laminar and the inertia term can be neglected [1].

(ii). Impermeable walls

$$\begin{aligned} &u^*=v^*=0 \qquad \text{for} \quad x^*=0,\ 0\le y^*\le 1,\\ &u^*=v^*=0 \qquad \text{for} \quad x^*=1,\ 0\le y^*\le 1. \end{aligned} \tag{2.13}$$

(iii). Exit

Stress free conditions expressed in the dimensionless form are imposed:

$$\tau_{yy}^*=2\frac{\partial v^*}{\partial y^*}=0 \qquad \text{for } y^*=1,\ 0\le x^*\le 1, \tag{2.14}$$

$$\tau_{yx}^*=\tau_{xy}^*=\left(\frac{\partial u^*}{\partial y^*}+\frac{\partial v^*}{\partial x^*}\right)=0 \qquad \text{for } y^*=1,\ 0\le x^*\le 1, \tag{2.15}$$

$$\tau_{xx}^*=2\frac{\partial u^*}{\partial x^*}=0 \qquad \text{for } y^*=1,\ 0\le x^*\le 1. \tag{2.16}$$

3 Multiscale modelling

To explain the multiscale finite element modelling based on the bubble functions, the multiscale variational and residual free bubble functions are presented.

3.1 Multiscale variational method

In the variational multiscale method, the unknowns are divided into functions having different scales. In a two-scale method this can be shown as

$$u_h = u_1 + u_b, \tag{3.1}$$

where u_b is known as the fine, sub-grid or unresolved scale and u_1 is known as coarse or resolved scale representing a standard finite element approximation polynomial (interpolation function). In the multiscale variational formulation which is developed by Hughes [4], for the sub-grid model we consider a Dirichlet problem as

$$\begin{cases} Lu_h = f, & \text{in } \Omega \text{ (domain)}, \\ u_h = g, & \text{on } \Gamma \text{ (boundary)}, \end{cases}$$

where L is a differential operator. Using the definition of a bilinear form as $a(\bullet,\bullet)$ the variational formulation for the above equation is

$$a(v_h,u_h) = (v_h,Lu_h),$$

where $(\bullet,\bullet)$ represents a scalar product. Let

$$\begin{cases} u_h = u_1 + u_b, \\ v_h = v_1 + v_b, \end{cases}$$

where we assume

$$u_b = v_b = 0 \qquad \text{on} \quad \Gamma_e \text{ (sub-domain boundary)}.$$

The variational formulation may be written as

$$a(v_h,u_h) = (v_h,f) \quad \text{or} \quad a(v_1+v_b,u_1+u_b) = (v_1+v_b,f).$$

It can be written as two sub-problems

$$a(v_b,u_1) + a(v_b,u_b) = (v_b,f), \tag{3.2}$$
$$a(v_1,u_1) + a(v_1,u_b) = (v_1,f). \tag{3.3}$$

The Euler-Lagrange equations of the first sub-problem is

$$\begin{cases} Lu_b = -(Lu_1 - f), & \text{in } \Omega_e \text{ (sub-domain)}, \\ u_b = 0, & \text{on } \Gamma_e \text{ (sub-domain boundary)}. \end{cases} \tag{3.4}$$

Multiscale variational method uses the Green's function approach to solve the above equation [4].

3.2 Residual free bubble function method

To solve (3.4), based on the residual free bubble function method the sub-grid scale is divided into two parts as

$$u_b = u_b^0 + u_b^f, \tag{3.5}$$

where u_b^0 and u_b^f are, respectively, solutions of the following equations [11]:

$$\begin{cases} Lu_b^0 = -Lu_1 & \text{in } \Omega_e, \\ u_b^0 = 0 & \text{on } \Gamma_e, \end{cases} \qquad \begin{cases} Lu_b^f = f & \text{in } \Omega_e, \\ u_b^f = 0 & \text{on } \Gamma_e. \end{cases} \tag{3.6}$$

Assuming that ϕ is a bubble shape function and ψ is a polynomial shape function, then Eq. (3.6) can be rewritten as

$$\begin{cases} L\phi_i = -L\psi_i & \text{in } \Omega_e, \\ \phi_i = 0 & \text{on } \Gamma_e, \end{cases} \tag{3.7}$$

where ψ_i and ϕ_i are functions associated with node i, Ω_e is the element domain and Γ_e is the element boundary. Hence

$$\begin{cases} L\phi_f = f & \text{in } \Omega_e, \\ \phi_f = 0 & \text{on } \Gamma_e, \end{cases} \tag{3.8}$$

and

$$u_h = u_1 + u_b = \sum_{i=1}^{n} u_i(\psi_i + \phi_i) + \phi_f, \tag{3.9}$$

where n is the number of nodes per element. To solve Eqs. (3.8) and (3.9) it is assumed that [15]

$$N_i = \psi_i + \phi_i. \tag{3.10}$$

For the Brinkman equation, operator L is defined as

$$L = \Delta - \frac{1}{Da}. \tag{3.11}$$

For a constant pressure drop assuming $f = p_d$, where p_d is the constant pressure drop (for penalty method used in this work, this assumption is not necessary)

$$p_d = -\frac{\partial p}{\partial y}. \tag{3.12}$$

Substituting Eq. (3.10) into Eq. (3.7), for a linear element on each node we have

$$\begin{cases} \frac{d^2N_1}{dx^2} - \frac{1}{Da}N_1 = 0 \quad \text{for } x \in [0-l], \\ N_1 = \psi_1 \Rightarrow \begin{cases} N_1(0) = 1, \\ N_1(l) = 0, \end{cases} \end{cases} \tag{3.13}$$

$$\begin{cases} \frac{d^2N_2}{dx^2} - \frac{1}{Da}N_2 = 0 \quad \text{for } x \in [0-l], \\ N_2 = \psi_2 \Rightarrow \begin{cases} N_2(0) = 0, \\ N_2(l) = 1, \end{cases} \end{cases} \tag{3.14}$$

where l is the characteristic element length and ψ_i is a linear shape function. The solution of the above equation gives bubble shape functions expressed in a local elemental coordinate system as

$$N_1=\frac{\sinh\sqrt{\frac{1}{Da}}(l-x)}{\sinh\sqrt{\frac{1}{Da}}l},\qquad N_2=\frac{\sinh\sqrt{\frac{1}{Da}}x}{\sinh\sqrt{\frac{1}{Da}}l}. \tag{3.15}$$

If Eq. (3.8) is solved, ϕ_f will be derived as

$$\phi_f=p_dDa(1-(N_1+N_2))=p_dDa\phi_b, \tag{3.16}$$

where ϕ_b is known as elemental bubble function [10].

4 Polynomial bubble functions

Hyperbolic functions in Eq. (3.15) can only be directly used if the integrals in the elemental equations are evaluated manually. However, this results in loss of flexibility and it is desirable to convert them into polynomials to make it possible to use quadrature methods in a finite element program. The Taylor series expansion can be used to express these functions as polynomials by truncating after a selected number of terms. For example, truncating after the second term third order polynomial bubble functions are derived as

$$N_1=\frac{(l-x)\left(1+\frac{(l-x^2)}{6Da}\right)}{l(1+\frac{1}{6Da}h^2)}=\frac{l-x}{l}-\frac{x(l-x)(2l-x)}{l(6Da+l^2)}, \tag{4.1}$$

$$N_2=\frac{x\left(1+\frac{1}{6Da}x^2\right)}{l(1+\frac{1}{6Da}l^2)}=\frac{x}{l}-\frac{x(l-x)(l+x)}{l(6Da+l^2)}. \tag{4.2}$$

In Eqs. (4.1) and (4.2) the second parts represent third order bubble functions

$$\begin{cases}\phi_1=\dfrac{x(l-x)(2l-x)}{l(6Da+l^2)},\\ \phi_2=\dfrac{x(l-x)(l+x)}{l(6Da+l^2)}.\end{cases} \tag{4.3}$$

Using a local coordinate system of $\xi(-1,1)$ the bubble functions are written as

$$\begin{cases}\phi_1=\dfrac{(1-\xi^2)(3-\xi)}{8\left(1+\frac{6Da}{l^2}\right)}=b(3-\xi)(1-\xi^2),\\ \phi_2=\dfrac{(1-\xi^2)(3+\xi)}{8\left(1+\frac{6Da}{l^2}\right)}=b(3+\xi)(1-\xi^2),\end{cases} \tag{4.4}$$

where $\xi=1-2x/l$, $b=\frac{1}{8}(1+6Da/l^2)^{-1}$, and l is a characteristic element length.

Using a similar procedure fifth order bubble enriched bilinear element can also be derived as

$$\begin{cases} \phi_1 = A[a(1-\xi^2)+b(1-\xi^2)(1-\xi)+c(1-\xi^2)^2+d(1-\xi^2)^2(1-\xi)], \\ \phi_2 = A[a(1-\xi^2)+b(1-\xi^2)(1+\xi)+c(1-\xi^2)^2+d(1-\xi^2)^2(1+\xi)], \end{cases} \tag{4.5}$$

where

$$A = \frac{1}{l\left(1+\frac{l^2}{6Da}+\frac{l^4}{120Da^2}\right)}, \quad a = \left(-\frac{l}{6Da}-\frac{l^3}{120Da^2}\right)\frac{l^2}{4},$$

$$b = \left(-\frac{l}{6Da}-\frac{3l^2}{120Da^2}\right)\frac{l^3}{8}, \quad c = \frac{2l^5}{1920Da^2}, \quad d = \frac{l^5}{3840Da^2}.$$

4.1 Static condensation

When the derived hyperbolic functions are approximated by the Taylor expansion, the resulting polynomial bubble functions are no longer residual free. In theory, any function which is zero at the element boundary is a bubble function. The fact that bubble functions disappear on element boundaries makes it possible to remove the equations that correspond to these functions from the set of elemental equations. This procedure is called static condensation [19]. In the residual free method, condensation takes place automatically for the derived bubble functions. Therefore, the bubble functions incorporation with Lagrangian shape functions takes place automatically. Bubble coefficients are calculated as a part of the condensation procedure. However, as an alternative other bubble functions can be used to incorporate with linear Lagrangian shape functions by means of the static condensation procedure. Two types of bubble functions are considered in this work. Based on derived polynomial in the residual free method and using optional elemental polynomial bubble functions. The structure of the bubble polynomials for the Brinkman equation can be considered as:

- Second order elemental bubble function:

$$\phi_b = (1-\xi^2), \tag{4.6}$$

- Fourth order elemental bubble function:

$$\phi_b = (1-\xi^2)+(1-\xi^2)^2, \tag{4.7}$$

- Sixth order elemental bubble function:

$$\phi_b = (1-\xi^2)+(1-\xi^2)^2+(1-\xi^2)^3. \tag{4.8}$$

According to the above polynomials it can be concluded that an m-th order elemental bubble function may be written as

$$\phi_b=(1-\xi^2)+(1-\xi^2)^2+\cdots+(1-\xi^2)^m=\sum_{q=1}^{m}(1-\xi^2)^q. \tag{4.9}$$

As another choice for the bubble functions we consider the following type of functions:

$$\phi_b=(1-\xi^{2n}),\quad n=1,2,\cdots. \tag{4.10}$$

To incorporate the bubble functions with ordinary shape functions, with respect to Eq. (3.1) we have

$$u_h=\psi_1u_1+\psi_2u_2+\phi_bu_b, \tag{4.11}$$

where ψ_i in this work is the Lagrangian linear shape function and ϕ_b is the polynomial bubble function. Using the static condensation procedure the bubble enriched one dimensional shape functions can be generally derived as

$$N_i=\psi_i+b\phi_b, \tag{4.12}$$

where b is the bubble coefficient and is derived during the implementation of the static condensation method (3.2).

4.2 Derivation of two dimensional bubble functions

Two dimensional bubble functions, required for practical implementations, can be derived using tensor products of one dimensional functions. The derived bubble functions are then incorporated into normal interpolation functions of bilinear Lagrangian elements to obtain shape functions of a bubble enriched bilinear element as

$$\begin{cases} N_1=\frac{1}{4}(1-\xi)(1-\eta)-b(1-\xi^2)(1-\eta^2),\\ N_2=\frac{1}{4}(1+\xi)(1-\eta)-b(1-\xi^2)(1-\eta^2),\\ N_3=\frac{1}{4}(1+\xi)(1+\eta)-b(1-\xi^2)(1-\eta^2),\\ N_4=\frac{1}{4}(1-\xi)(1+\eta)-b(1-\xi^2)(1-\eta^2), \end{cases} \tag{4.13}$$

where

$$b=\frac{1}{8(0.2+2Dal^{-2})}, \tag{4.14}$$

which is calculated during the implementation of the static condensation method. Here l is a characteristic length of the element. Using the same procedure forth order bubble enriched bilinear elements can be derived as

$$\begin{cases} N_1=\frac{1}{4}(1-\xi)(1-\eta)-b[(1-\xi^2)(1-\eta^2)+(1-\xi^2)^2(1-\eta^2)^2],\\ N_2=\frac{1}{4}(1+\xi)(1-\eta)-b[(1-\xi^2)(1-\eta^2)+(1-\xi^2)^2(1-\eta^2)^2],\\ N_3=\frac{1}{4}(1+\xi)(1+\eta)-b[(1-\xi^2)(1-\eta^2)+(1-\xi^2)^2(1-\eta^2)^2],\\ N_4=\frac{1}{4}(1-\xi)(1+\eta)-b[(1-\xi^2)(1-\eta^2)+(1-\xi^2)^2(1-\eta^2)^2], \end{cases} \tag{4.15}$$

where

$$b=\frac{1}{8(0.386+3.905Dal^{-2})}. \tag{4.16}$$

Any higher order bubble enriched bilinear element can be derived similarly.

If the n-th order bubble function (4.10) is used the two dimensional bubble enriched bilinear shape functions can be written as

$$\begin{cases} N_1=\frac{1}{4}(1-\xi)(1-\eta)-b(1-\xi^{2n})(1-\eta^{2n}), \\ N_2=\frac{1}{4}(1+\xi)(1-\eta)-b(1-\xi^{2n})(1-\eta^{2n}), \\ N_3=\frac{1}{4}(1+\xi)(1+\eta)-b(1-\xi^{2n})(1-\eta^{2n}), \\ N_4=\frac{1}{4}(1-\xi)(1+\eta)-b(1-\xi^{2n})(1-\eta^{2n}), \end{cases} \tag{4.17}$$

where b is represented as

$$b=\frac{l}{2Da}\frac{2n}{2n+1}\left(\frac{16n^2}{(4n-1)l}+\frac{8n^2l}{(4n+1)(2n+1)Da}\right)^{-1}. \tag{4.18}$$

4.3 Elimination of inter-element boundary integrals

When bubble functions are applied the inter-element boundary integrals are not automatically eliminated during the assembly of elemental equations. This problem does not become apparent in the one dimensional case as the boundary integrals are reduced to simple nodal flux terms. The variational formulation for the Brinkman equation, after application of Green's theorem is

$$\left(\frac{1}{Da}u_h,v_1\right)+(\nabla u_h,\nabla v_1)=(p_d,v_1). \tag{4.19}$$

Substitution from Eq. (3.1) gives

$$\left(\frac{1}{Da}u_h,v_1\right)+(\nabla u_1,\nabla v_1)+(\nabla u_b,\nabla v_1)=(p,v_1). \tag{4.20}$$

If v_1 is a linear test function (weight function), then according to Green's theorem [20]:

$$(\nabla v_1,\nabla\phi)_{\Omega_e}=-(\Delta v_1,\phi)_{\Omega_e}+(\nabla v_1,\phi)_{\Gamma_e}=0, \tag{4.21}$$

where ϕ is a bubble function. Therefore Eq. (4.20) is reduced to

$$\left(\frac{1}{Da}u_h,v_1\right)+(\nabla u_1,\nabla v_1)=(p,v_1). \tag{4.22}$$

As can be seen the bubble function does not affect the Laplacian term in the Brinkman equation and therefore no boundary integral due to the bubble function exists.

5 Finite element scheme

There are a variety of different finite element schemes that can be used for the solution of the governing equations of porous flow regimes. The finite element scheme used in the present work is based on the continuous penalty technique [21]. This technique is in essence similar to the "Lagrange Multiplier Method" used for the solution of differential equations subject to a constraint. Here the continuity equation (i.e. the incompressibility condition) is regarded as a constraint for the equation of motion. Therefore instead of solving the governing flow equations as a system of three PDEs the pressure in the components of the equation of motion is replaced by a multiplier (called penalty parameter) times the continuity equation. This gives a more compact set of working equations with components of the velocity as the remaining unknowns. Additionally, elimination of the pressure from the equation of motion automatically satisfies the basic numerical stability condition for the simulation of incompressible flows, known as the LBB criteria. The mathematical theory underpinning the development of LBB criterion is somewhat obscure [19]. However, it can be readily observed that the absence of a pressure term in the incompressible continuity equation makes the possibility of a mismatch between approximations used to satisfy the equations of motion and continuity almost inevitable in any numerical solution of a system of PDEs with velocity and pressure as the prime unknowns. It has been proved that for the bubble enriched bilinear elements the LBB condition is still satisfied [22]. If the continuous penalty scheme is used, after representing the unknowns based on the trial functions the governing equations can be written as

$$\int_{\Omega_e} W_i \left[\frac{\partial}{\partial x^*} \lambda_0 \left(\frac{\partial}{\partial x^*} \sum_{j=1}^{n} N_j u_j^* + \frac{\partial}{\partial y^*} \sum_{j=1}^{n} N_j v_j^* \right) - \frac{1}{Da} \sum_{J=1}^{n} N_j u_j^* + \left(\frac{\partial^2}{\partial x^{*2}} \sum_{j=1}^{n} N_j u_j^* + \frac{\partial^2}{\partial y^{*2}} \sum_{j=1}^{n} N_j u_j^* \right) \right] dx^* dy^* = 0, \tag{5.1}$$

$$\int_{\Omega_e} W_i \left[\frac{\partial}{\partial y^*} \lambda_0 \left(\frac{\partial}{\partial x^*} \sum_{j=1}^{n} N_j u_j^* + \frac{\partial}{\partial y^*} \sum_{j=1}^{n} N_j v_j^* \right) - \frac{1}{Da} \sum_{J=1}^{n} N_j v_j^* + \left(\frac{\partial^2}{\partial x^{*2}} \sum_{j=1}^{n} N_j v_j^* + \frac{\partial^2}{\partial y^{*2}} \sum_{j=1}^{n} N_j v_j^* \right) \right] dx^* dy^* = 0, \tag{5.2}$$

where W_i is a weight function and is equal to the Lagrangian shape function ψ_i in the standard Galerkin method and N_j is the bubble enriched shape function.

The penalty parameter λ_0 should be chosen to be large enough so that the mass continuity is satisfied [23], however, at the same time it should not be so large that working equations of the scheme become ill-conditioned (i.e. physically important terms in them become insignificant). Therefore the selection of this value requires numerical experi-

ments. In the present work a value of $\lambda_0 = 10^{10}$ is found to generate accurate results for the benchmark problems and is used in all of the simulations.

As shown in Eqs. (5.1) and (5.2) the use of the penalty method results in the derivation of working equations in a compact form in which the pressure is eliminated from the set. Therefore the calculation of pressure must be carried out in a separate step after the determination of the velocity field. In this study the well known variational recovery method [23] is used to calculate the pressure fields.

Eqs. (5.1) and (5.2) can be used corresponding to a total of n interpolation functions to obtain n equations and a system of $n \times n$ equations is constructed. Using matrix notation in [23] this system is written as

$$\begin{bmatrix} A_{ij}^{11} & A_{ij}^{12} \\ A_{ij}^{21} & A_{ij}^{22} \end{bmatrix} \begin{Bmatrix} u_j^* \\ v_j^* \end{Bmatrix} = \begin{Bmatrix} B_j^1 \\ B_j^2 \end{Bmatrix}, \tag{5.3}$$

where

$$A_{ij}^{11} = \int_{\Omega_e} \left[(\lambda_0 + 1) \left(\frac{\partial W_i}{\partial x^*} \frac{\partial N_j}{\partial x^*} \right) + \frac{\partial W_i}{\partial y^*} \frac{\partial N_j}{\partial y^*} + \frac{1}{Da} W_i N_j \right] dx^* dy^*,$$

$$A_{ij}^{12} = \int_{\Omega_e} \lambda_0 \frac{\partial W_i}{\partial x^*} \frac{\partial N_j}{\partial y^*} dx^* dy^*, \qquad A_{ij}^{21} = \int_{\Omega_e} \lambda_0 \frac{\partial W_i}{\partial y^*} \frac{\partial N_j}{\partial x^*} dx^* dy^*,$$

$$A_{ij}^{22} = \int_{\Omega_e} \left[(\lambda_0 + 1) \left(\frac{\partial W_i}{\partial y^*} \frac{\partial N_j}{\partial y^*} \right) + \frac{\partial W_i}{\partial x^*} \frac{\partial N_j}{\partial x^*} + \frac{1}{Da} W_i N_j \right] dx^* dy^*,$$

$$B_j^1 = \int_{\Gamma_e} W_i \left\{ \left[\lambda_0 \left(\frac{\partial u^{*e}}{\partial x^*} + \frac{\partial v^{*e}}{\partial y^*} \right) + \frac{\partial u^{*e}}{\partial x^*} \right] n_x + \left(\frac{\partial u^{*e}}{\partial y^*} \right) n_y \right\} d\Gamma_e,$$

$$B_j^2 = \int_{\Gamma_e} W_i \left\{ \left(\frac{\partial v^{*e}}{\partial x^*} \right) n_x + \left[\lambda_0 \left(\frac{\partial u^{*e}}{\partial x^*} + \frac{\partial v^{*e}}{\partial y^*} \right) + \frac{\partial v^{*e}}{\partial y^*} \right] n_y \right\} d\Gamma_e.$$

A system of weighted residual equations should be derived for each element in the domain. This is obviously not convenient. However, by using an elemental coordinate system rather than the global coordinates the uniformity of the matrix Eq. (5.3) can be preserved. This is achieved via using isoparametric mapping of elements of the global mesh into a master element where all the calculations are carried out [24]. In addition, a natural coordinate system such as $-1 \leq \xi, \eta \leq 1$ can be used within the master element to enable the evaluation of all integrals within its domain by Gauss quadrature method [25].

Repeated application of the above procedure to each element in the computational mesh leads to the construction of elemental weighted residual equations written in matrix notations. Subsequent assembly of these equations over the common nodes between elements provides a system of global algebraic equations. Imposition of all boundary conditions into the assembled set of working equations renders the global system determinate which is then solved using a solution technique such as the Gaussian elimination

method. A computationally efficient version of this method which relies on bit by bit reducing of the global system to upper triangular form according to an advancing front is used in the present work [26].

6 Analytical solution

To evaluate the accuracy of the numerical solutions obtained using bubble enriched elements they are compared with an analytical solution. The dimensionless Brinkman equation in one dimension corresponding to a constant pressure drop can be written as

$$\begin{cases} \dfrac{d^2v^*}{dx*^2}-\dfrac{1}{Da}v^*+p_d^*=0, \\ v^*=0, \quad \text{at} \quad x^*=0 \ \text{ or } \ x^*=1, \end{cases} \tag{6.1}$$

where

$$p_d^*=-\frac{\partial P^*}{\partial y^*}.$$

Solution of the above equation gives

$$v^*=\frac{p_d^*Da(e^{-\alpha}-1)}{(e^{\alpha}-e^{-\alpha})}(e^{\alpha x^*}-e^{-\alpha x^*})+p_d^*Da(1-e^{-\alpha x^*}),$$

where

$$\alpha=\sqrt{\frac{1}{Da}}.$$

To calculate pressure so that the consistency of the solution with numerical results is preserved, the average velocity has to be equal to the input plug flow velocity. In the present domain it is written as

$$\int_0^1 v^*dx^*=v_0^*.$$

Solution of the above equation gives

$$p_d^*=\frac{1}{Da}v_0^*\left[1+\frac{1}{\alpha}\left(e^{-\alpha}-1\right)\left(1+\frac{Da(e^{\alpha}-e^{-\alpha}-2)}{e^{\alpha}-e^{-\alpha}}\right)\right]^{-1}. \tag{6.2}$$

Excess pressure loss due to the entrance region can be neglected [17].

7 Results

To investigate the effect of using bubble enriched finite elements we have conducted a series of numerical experiments. These experiments cover a wide range of Darcy parameter (permeability) using both ordinary Lagrangian elements and bubble enriched

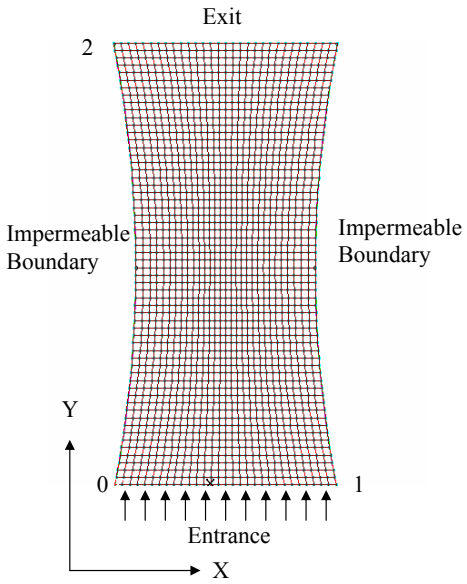

Figure 2: Flow domain and boundaries with variable cross section width and curved sides (domain 2).

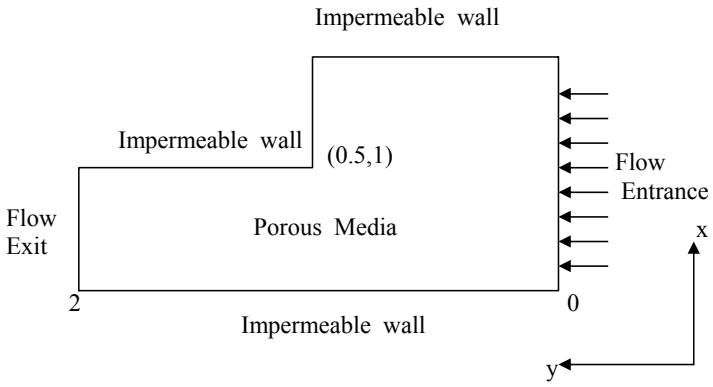

Figure 3: Sudden contraction flow domain (domain 3).

elements. The performance of different types of bubble functions are studied. In order to be able to use bubble enriched elements flexibly, an in-house developed computer code in FORTRAN was used to carry out the finite element simulations. In all of the presented simulations 4-noded Lagrangian elements are used. Three different domains are used to evaluate the developed multi-scale method. A rectangular domain with constant mesh density (30×30 rectangular elements) for numerical model validation (domain 1, Fig. 1), a contracting and expanding domain with curvilinear boundaries (30×60 mesh density) to study the effects of deviation from the most simple geometry and element (domain 2, Fig. 2) and a sudden contracting domain (domain 3, Fig. 3) with constant mesh density similar to domain 1.

In order to discretise the domain with curved boundaries shown in Fig. 2 the routine procedure of isoparametric mapping is used [23]. As the results shown here proves isoparametric mapping (elements) can be used in the context of bubble enriched discretisations without any change to the normal implementation of the finite element method.

The first series of experiments are performed in domain 1 to compare the results of different types of bubble functions and evaluate the accuracy with respect to analytical solution. The comparison of the bubble function is carried out on this domain and on the other domains only the bubble functions which are represented in Eqs. (4.13) and (4.15) are evaluated. Fig. 1 shows the domain and its boundaries. Fig. 4 demonstrates a comparison between the 3*rd* and 5*th*-order bubble functions derived directly from residual free method at Da=10^{-5}. As Fig. 4 shows ordinary elements fail to generate a stable and accurate solution while bubble enriched elements give stable and, in comparison with analytical solution, accurate results. The accuracy increases when 5*th*-order bubble is used. At other Darcy parameters the same trend is observed , however, to avoid repetition they are not shown here. Fig. 5 shows the results for 2*nd* and 4*th*-order bubble functions which are represented in Eqs. (4.13) and (4.15). It is seen that the same results as Fig. 4 is achieved and by increasing the order of the bubble function the accuracy of the numerical solution increases. The results for the bubble functions in Eq. (4.17) are represented in Fig. 6. As the results show by increasing the degree of the bubble function the accuracy of the numerical solution decreases while the solution is stable. These results show that although theoretically any bubble function has stabilizing effect on the solution but it is not necessarily accurate.

Figs. 7-11 show the results for dimensionless velocity at different cross sections of the domain 2. In this domain the boundary conditions are similar to domain 1, i.e. plug flow at the inlet, no-slip boundary conditions at the solid walls and stress free conditions at the outlet of the domain. Fig. 7 shows the result of 2*nd*-order bubble function at y*=0.667 and Da=10^{-4}. It is obvious that the bubble enriched element gives a stable solution. Fig. 8 shows the same result at y*=1.33. Therefore, for both contracting and expanding sections with curvilinear boundaries the bubble enriched elements give stable results. This implies that the mapping error between the quadrilateral elements with curved sides into master element has no deteriorating effect on the performance of the developed method. Figs. 9-11 show the results at y*=1 and different Darcy parameters. By decreasing the Darcy parameter, instability increases for ordinary elements, but using bubble functions the solution remains stable and accurate. As expected, the 4*th*-order bubble function gives more accurate results in comparison with the 2*nd*-order bubble function. Fig. 12 shows the dimensionless pressure field in domain 2 which matches the theoretically expected result.

An abruptly contracting domain, which includes a point of singularity, is also considered. Fig. 3 shows the domain and its boundaries discretised using the same mesh density as the rectangular domain shown in Fig. 1. The ratio of contraction is 2:1. Simulations are based on using the same boundary conditions as for the rectangular domain. Fig. 13 shows the 2D image of the flow field obtained using 2*nd*-order bubble functions. Fig. 14

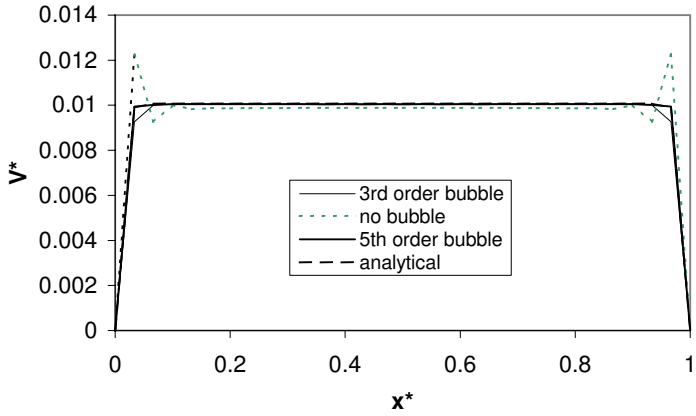

Figure 4: Comparison of the numerical and analytical velocity profiles at mid-height cross section for Da=10^{-5}.

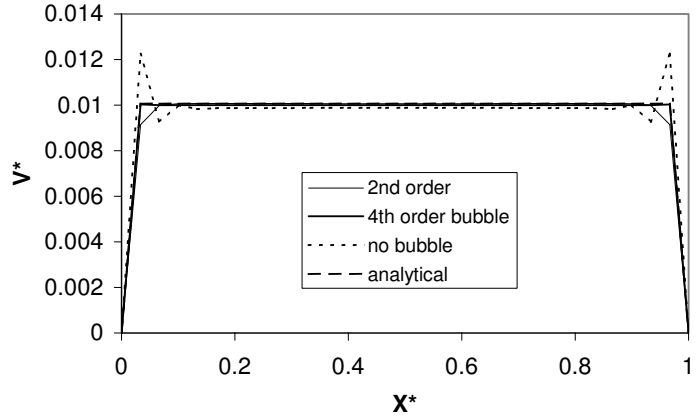

Figure 5: Velocity profile comparison at mid-height cross section and Da=10^{-5} for domain 1.

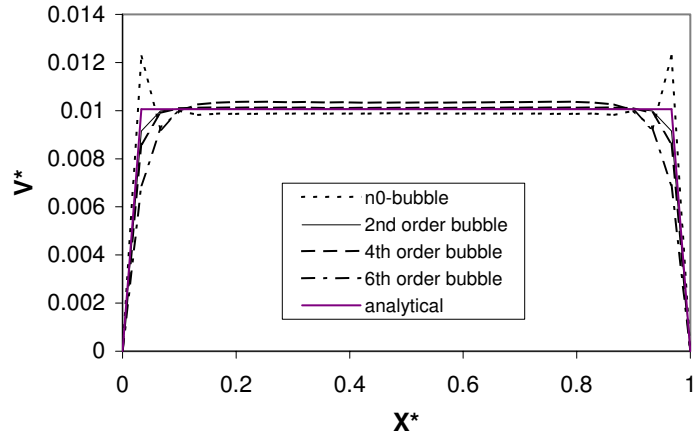

Figure 6: Velocity profile comparison at mid-height cross section and Da=10^{-5} for domain 1 using the bubble functions of the form $\phi_b=(1-\xi^{2n})(1-\eta^{2n})$.

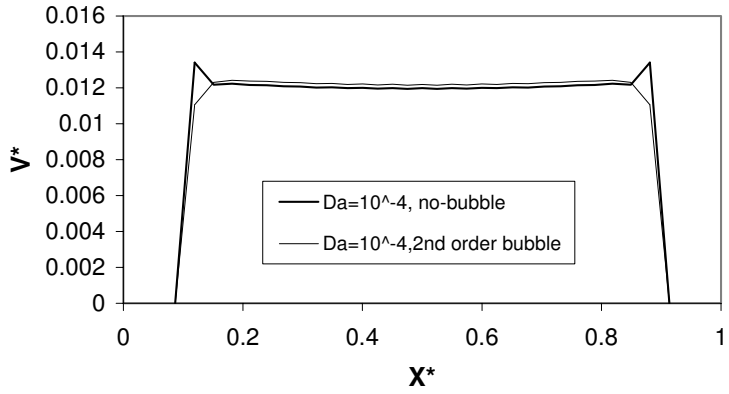

Figure 7: Dimensionless velocity at the cross section $y=0.667$ (domain 2) for Da=10^{-4} and $2nd$-order bubble function.

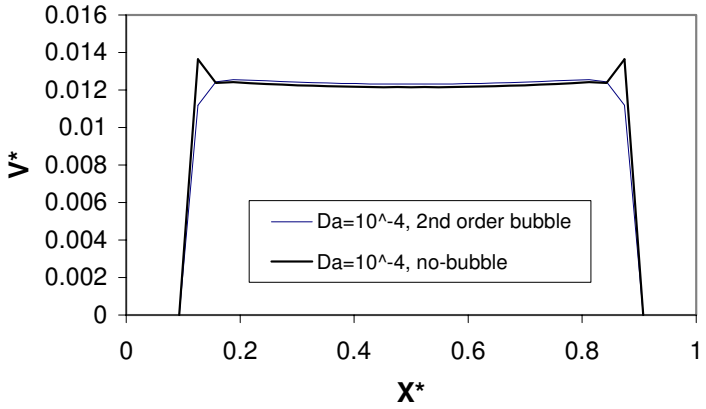

Figure 8: Dimensionless velocity at the cross section $y=1.33$ (domain 2) for Da=10^{-4} and $2nd$-order bubble function.

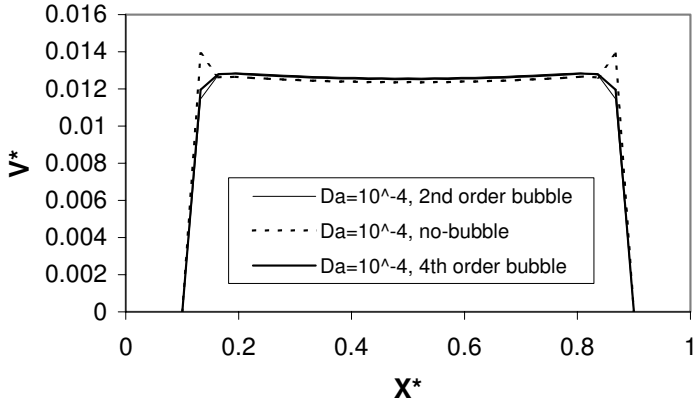

Figure 9: Dimensionless velocity at the cross section $y=1$ (domain 2). Comparison at Da=10^{-4} for $2nd$-order and $4th$-order bubble functions.

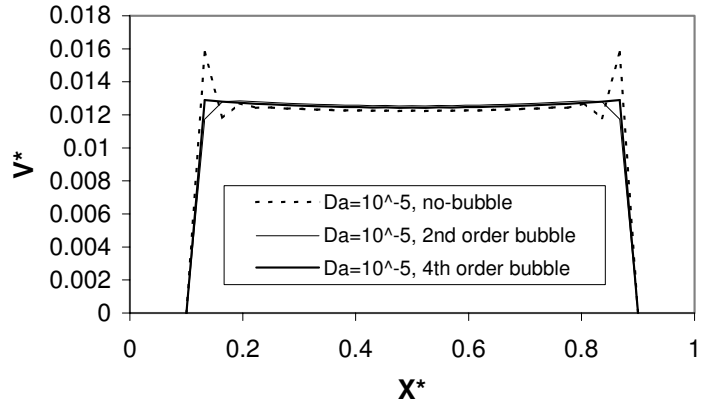

Figure 10: Dimensionless velocity at the cross section $y=1$ (domain 2). Comparison at Da=10^{-5} for $2nd$-order and $4th$-order bubble functions.

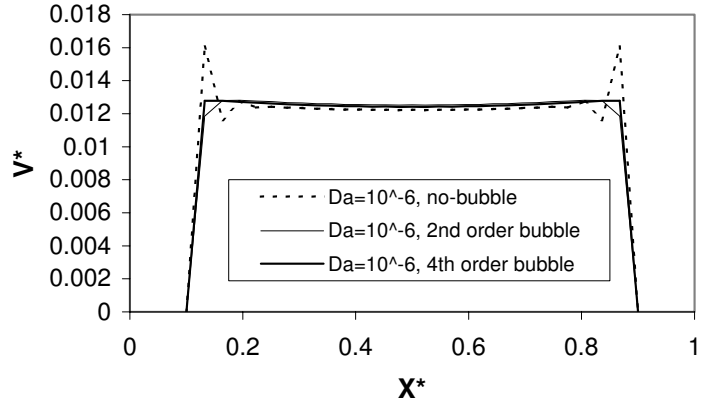

Figure 11: Dimensionless velocity at the cross section $y=1$ (domain 2). Comparison at Da=10^{-6} for $2nd$-order and $4th$-order bubble functions.

represents the dimensionless velocity at the cross section corresponding to y*=0.5 and Da=10^{-4}. Using Da=10^{-5}, as Fig. 15 shows, some slight instability through the whole cross section is observed. These oscillations are eliminated using $2nd$-order bubble enriched elements. The pressure field corresponding to Da=10^{-4} is illustrated in Fig. 16 which matches the theoretically expected result.

8 Conclusion

In the present paper different types of bubble functions are evaluated in the simulation of flow in highly permeable porous media using the Brinkman equation. The derivation of two dimensional bubble enriched shape functions, their implementation and performances are presented. Static condensation method is used to incorporate the bubble func-

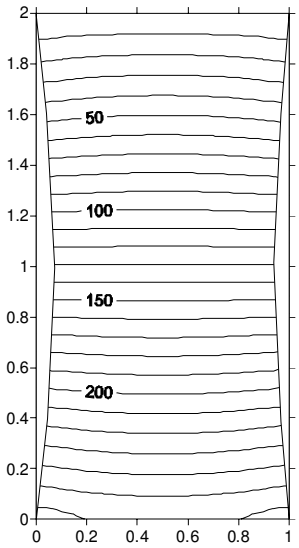

Figure 12: Dimensionless pressure field for Da=10^{-4} in domain 2.

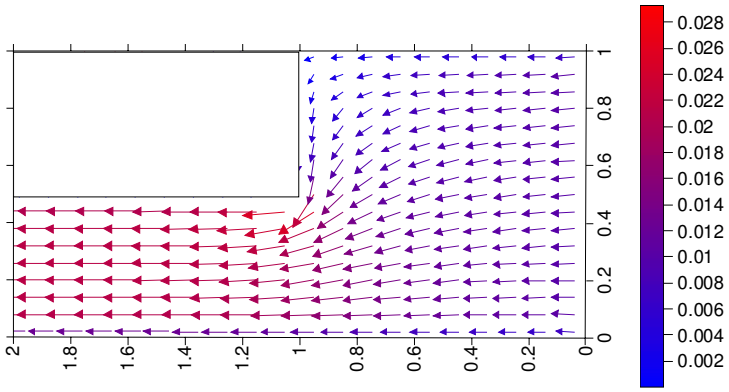

Figure 13: 2D image of the flow field for domain 3.

tions with the ordinary shape functions to perform a multiscale finite element scheme. The numerical results show that those bubble functions which are derived directly by residual free method or have the same structure yield stable and accurate solution. For other kind of the bubble function the solution is stable but the level of accuracy can not be guaranteed. The successful bubble functions are used in other domains rather than the simple rectangular domain. Discretisations using bubble enriched elements are shown to generate stable accurate simulations for domains involving curved boundaries and abrupt changes of geometry. Although the presented method was used to model the flow in highly permeable porous media it should be considered as a general technique for multiscale finite element solution of transport phenomena involving multiscale behaviour.

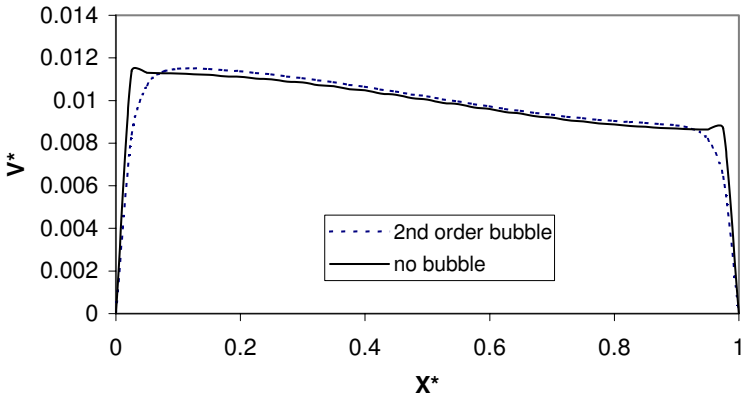

Figure 14: Dimensionless velocity profile comparison cross section y=0.5 and Da=10^{-4} for domain3.

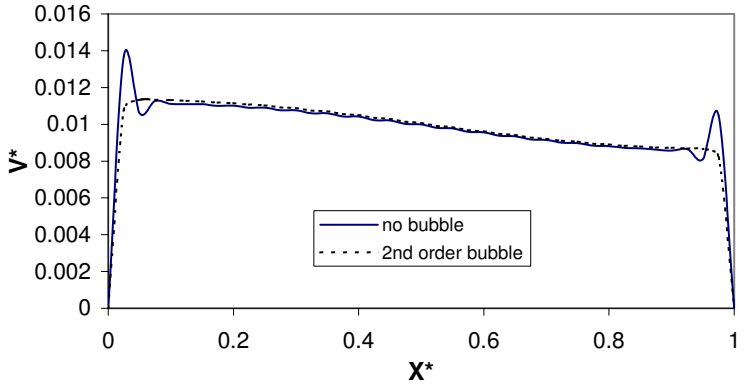

Figure 15: Dimensionless velocity profile comparison cross section y=0.5 and Da=10^{-5} for domain3.

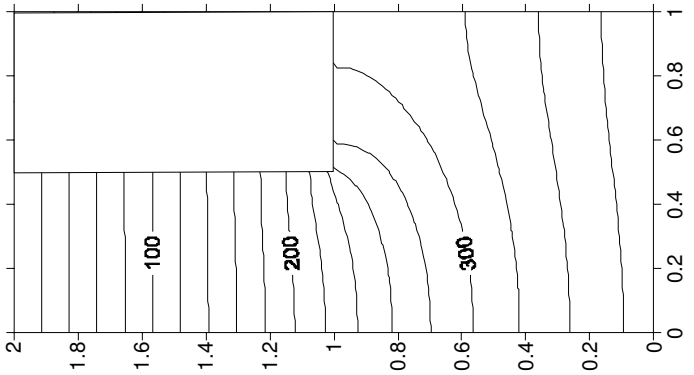

Figure 16: 2D image of the dimensionless pressure field at Da=10^{-4} for domain 3.

References

[1] D. A. Nield and A. Bejan, Convection in Porous Media, Springer-Verlag, New York, 1992.
[2] M. Parvazinia, V. Nassehi, R. J. Wakeman and M. H. R. Ghoreishy, Finite element modelling of flow through a porous medium between two parallel plates using the Brinkman equation, Transport Porous Media, 2006, in press.
[3] J. Donea and A. Huerta, Finite Element Methods for Flow Problems, John Wiely & Sons, Chichester, 2003.
[4] T. J. R. Hughes, Multi-scale phenomena, Green's functions, the Dirichlet-to-Neumann formulation, subgrid scale models, bubbles and the origins of stabilized methods, Comput. Method. Appl. Mech. Engrg., 127 (1995), 381-401.
[5] T. J. R. Hughes and J. Stewart, A space time formulation for multi-scale phenomena, Comput. Method. Appl. Mech. Engrg., 74 (1996), 217-229.
[6] V. Gravimier, W. A. Wall and E. Ramm, A three-level finite element method for the instationary incompressible Navier-Stokes equations, Comput. Method. Appl. Mech. Engrg., 193 (2004), 1323-1366.
[7] F. Brezzi, M. Bristeau, L. P. Franca, M. Mallet and G. Roge, A relationship between stablized finite element methods and the Galerkin method with bubble functions. Comput. Method. Appl. Mech. Engrg., 96 (1992), 117-129.
[8] C. Baiocchi, F. Brezzi and L. P. Franca, Virtual bubbles and Galerkin-least-squares type methods, Comput. Method. Appl. Mech. Engrg., 105 (1993), 125-141.
[9] L. P. Franca, T. J. R. Hughes and R. Stenberg, Stabilized finite element methods for the Stokes problem, in: R. A. Nicolaides and M. D. Gunzberger (Eds.), Incompressible Fluid Dynamics-Trends and Advances, Cambridge University Press, Cambridge, 1993.
[10] F. Brezzi, L. P. Franca, T. J. R. Hughes and A. Russo, $b=\int g$, Comput. Method. Appl. Mech. Engrg., 145 (1997), 392-339.
[11] F. Brezzi, L. P. Franca and A. Russo, Further considerations on residual-free bubbles for advective-diffusive equations, Comput. Method. Appl. Mech. Engrg., 166 (1998), 25-33.
[12] L. P. Franca, C. Farhat, A. P. Macedo and M. Lesoinne, Residual free bubbles for Helmholtz equation, Comput. Method. Appl. Mech. Engrg., 40 (1997), 4003-4009.
[13] L. P. Franca and A. Russo, Deriving upwinding, mass lumping and selective reduced integration by residual free bubbles, Appl. Math. Lett., 9 (1996), 83-88.
[14] L. P. Franca and A. Russo, Unlocking with residual-free bubbles, Comput. Method. Appl. Mech. Engrg., 142 (1997), 361-364.
[15] L. P. Franca and A. Russo, Mass lumping emanating from residual free bubbles, Comput. Method. Appl. Mech. Engrg., 142 (1997), 353-360.
[16] C. T. Hsu and P. Cheng, The Brinkman model for natural convection about a semi-infinite vertical flat plate in a porous medium, Int. J. Heat Mass Tran., 28 (1985), 683-697.
[17] M. Kaviany, Non-Darcian effects on natural convection in porous media confined between horizontal cylinders, Int. J. Heat Mass Tran., 29 (1986), 1513-1519.
[18] F. M. Allan and M. H. Hamdan, Fluid mechanics of the interface region between two porous layers, Appl. Math. Comput., 128 (2002), 37-43.
[19] K. J. Bathe, Finite Element Procedures, Prentice Hall, New Jersey, 1996.
[20] L. P. Franca and C. Farhat, Bubble functions prompt unusual stabilized finite element methods, Comput. Method. Appl. Mech. Engrg., 123 (1995), 299-308.
[21] J. F. T. Pittman, Finite elements for field problems, in: C. L. Tucker III (Ed.), Computer Modelling for Polymer Processing, Hanser Publishers, Munich, 1989.

[22] W. Bai, The quadrilateral 'Mini' finite element for the Stokes problem, Comput. Method. Appl. Mech. Engrg., 143 (1997), 41-47.
[23] V. Nassehi, Practical Aspects of Finite Element Modelling of Polymer Processing, John Wiely & Sons, Chichester, 2002.
[24] O. C. Zienkiewicz and R. L. Taylor, The Finite Element Method, McGraw-Hill, London, 1994.
[25] C. F. Gerald and P. O. Wheatley, Applied Numerical Analysis, Addison-Wesley, London, 1984.
[26] B. M. Irons, A frontal solution for finite element analysis, Int. J. Numer. Meth. Engrg., 2 (1970), 5-32.